THE JOURNAL OF BIOLOGICAL CHEMISTRY VOL. 290, NO. 13, pp. 8360–8372, March 27, 2015

Direct Interactions with the Integrin β1 Cytoplasmic Tail Activate the Abl2/Arg Kinase*

Received for publication, January 15, 2015 Published, JBC Papers in Press, February 18, 2015, DOI 10.1074/jbc.M115.638874

Mark A. Simpson[‡1,2], William D. Bradley[‡1,3], David Harburger[§], Maddy Parsons[¶4], David A. Calderwood[§‖5], and Anthony J. Koleske[‡6]**

*From the Departments of [‡]Molecular Biophysics and Biochemistry, [§]Pharmacology, [‖]Cell Biology, and **Neurobiology, Yale University, New Haven, Connecticut 06510 and the [¶]Randall Division of Cell and Molecular Biophysics, Kings College, London WC2R 2LS, United Kingdom*

Background: Integrin adhesion drives Arg kinase activity-dependent changes in cell motility and morphogenesis.
Results: Arg activation is enhanced upon engaging two distinct interfaces in the integrin β1 tail.
Conclusion: The integrin β1-Arg signaling axis is driven by direct interactions.
Significance: Direct interactions with the integrin β1 tail mediate Arg kinase activity to promote changes in cell shape and motility.

Integrins are heterodimeric α/β extracellular matrix adhesion receptors that couple physically to the actin cytoskeleton and regulate kinase signaling pathways to control cytoskeletal remodeling and adhesion complex formation and disassembly. β1 integrins signal through the Abl2/Arg (Abl-related gene) nonreceptor tyrosine kinase to control fibroblast cell motility, neuronal dendrite morphogenesis and stability, and cancer cell invasiveness, but the molecular mechanisms by which integrin β1 activates Arg are unknown. We report here that the Arg kinase domain interacts directly with a lysine-rich membrane-proximal segment in the integrin β1 cytoplasmic tail, that Arg phosphorylates the membrane-proximal Tyr-783 in the β1 tail, and that the Arg Src homology domain then engages this phosphorylated region in the tail. We show that these interactions mediate direct binding between integrin β1 and Arg *in vitro* and in cells and activate Arg kinase activity. These findings provide a model for understanding how β1-containing integrins interact with and activate Abl family kinases.

Integrins are heterodimeric cell surface receptors that transduce signals from the extracellular matrix to the actin cytoskeleton to promote changes in cell shape and motility (1). Abl family nonreceptor tyrosine kinases, comprised of Abl1/Abl and Abl2/Arg (Abl-related gene) in vertebrates, mediate changes in cell shape and movement in response to integrin-mediated adhesion. This occurs through integrin adhesion driven Abl- and Arg-dependent phosphorylation of key cytoskeletal substrates such as p190RhoGAP, cortactin, and the adaptor protein CrkII (2–6).

Integrin β1 interacts functionally with Arg to control cell edge protrusion in spreading fibroblasts (5, 7), dendrite and dendritic spine stabilization in neurons (8, 9), and invadopodial maturation in invasive breast cancer cells (10). We have previously shown that this integrin-dependent adhesion pathway drives Arg kinase-dependent directed cell migration and cell edge dynamics. Importantly, this process is dependent upon Arg kinase activity as a point mutation rendering Arg kinase inactive, or pharmacological inhibition of Arg kinase activity disrupts these cellular behaviors (5, 11). Similarly, we have shown that inhibiting Arg kinase activity disrupts neurite branching in cultured cortical neurons following integrin-mediated adhesion to laminin. The laminin-binding integrin α3β1 receptor also acts through an Arg-p190RhoGAP-RhoA GTPase cascade to regulate hippocampal dendrite arbor stability (8, 9, 12). Finally, we have previously reported that Arg, but not Abl, is enriched in invadopodia of highly metastatic breast cancer cells, that its kinase activity is required for efficient matrix degradation and invasion, and that integrin β1 signaling through Arg is critical for these processes (10, 13).

Despite these central roles for integrin β1-Arg interactions in cell morphogenesis and motility, the molecular mechanism by which integrins control Abl family kinase activation is unknown. Here we report the mechanism by which integrin β1 interacts with and activates Arg kinase. We find that two distinct interfaces mediate direct binding of integrin β1 with Arg *in vitro* and in cells and promote Arg kinase activation.

EXPERIMENTAL PROCEDURES

Molecular Cloning—Full-length Arg and Arg kinase domains were cloned into pFastBac (Invitrogen) expression vectors as previously described (8). GST-Arg-SH3-SH2, GST-Arg-SH2, GST-β1 tails, and GST-CrkII constructs were cloned as previously described (8, 14–16). The talin F3 subdomain was cloned into pGEX-6P-1 from a talin cDNA. For the FRET-FLIM studies, mutants were generated in β1-GFP constructs previously cloned as described (17). Arg-mCherry or Arg-RFP constructs

* This work was supported, in whole or in part, by National Institutes of Health Grants CA133346 and GM100411 (to A. J. K.).
[1] These authors contributed equally to this work.
[2] Supported by T32GM007223-40 from NIGMS, National Institutes of Health and American Heart Association Founders Affiliate Predoctoral Fellowship Award #12PRE12080140.
[3] Present address: Constellation Pharmaceuticals, Cambridge, MA 02142.
[4] Supported by the Royal Society.
[5] Supported by National Institutes of Health Grant RO1 GM068600.
[6] To whom correspondence should be addressed: Dept. of Molecular Biophysics and Biochemistry, Yale University, P.O. Box 208024, New Haven, CT 06520-8024. E-mail: anthony.koleske@yale.edu.

were cloned into pN1-eGFP (Clontech) or pK1 vectors where eGFP was replaced with mCherry or RFP (5). Cre was cloned into the pBABE-Hygro vector from a Cre cDNA.

Cell Culture and Antibodies—Experiments were performed in HEK 293T-derived Phoenix cells (ATCC, Manassas, VA), or WT ($\beta1^{flox/flox}$) or *integrin* $\beta1^{-/-}$ mouse 3T3 fibroblast lines. WT ($\beta1^{flox/flox}$) murine embryonic fibroblast cells were spontaneously immortalized using the 3T3 protocol by passaging at 3.75×10^5 cells/10-cm dish every 3 days for up to 20 passages as described previously (18). *Integrin* $\beta1^{-/-}$ fibroblasts were generated from these WT 3T3 cells by retroviral infection with Cre retrovirus, followed by selection with 200 or 500 μg/ml hygromycin for 7 days. β1 knock-out was confirmed by immunoblotting for β1. Cells were cultured at 37 °C in 5% CO_2 in DMEM medium supplemented with 10% FBS. The following antibodies were used for this study: phosphotyrosine (4G10; Upstate/Millipore, Billerica, MA, or affinity-purified from hybridomas), GST (Rockland, Boyertown, PA, or purified from hybridomas), Tyr(P)-783 β1 integrin (Abcam, Cambridge, MA), integrin β1 (BD Biosciences, San Jose, CA), cortactin (4F11; purified from hybridomas), Arg (Ar11, Ar19; purified from hybridomas, a kind gift from Peter Davies), and actin (C4; Millipore).

Recombinant Protein Purification—Recombinant baculovirally expressed His-Arg and His-Arg kinase domain were purified from High Five (Life Technologies) insect cells as previously described (8, 15). GST-Arg-SH3-SH2, GST-Arg-SH2, and GST-talin-F3 were expressed from pGEX-6P-1 and purified from bacterial cells. GST tags were cleaved using PreScission Protease (GE Healthcare) as previously described (8). GST-β1 constructs and GST-CrkII were expressed from pGEX-4T-1 and purified from bacterial cells as previously described (8, 15, 19). Before use in assays, all proteins were buffer-exchanged into assay buffer containing 25 mM Hepes, pH 7.25, 100 mM NaCl, 5% glycerol, 0.01% Triton X-100, and 1 mM DTT.

Cross-linking of Recombinant Proteins to Beads—AminoLink (Thermo Scientific, Waltham, MA) beads were used to covalently link Arg and talin-F3 constructs following purification as described previously (8). Briefly, proteins were buffer-exchanged into 3.65× PBS before gently rotating with AminoLink beads overnight. Sodium cyanoborohydride was added to catalyze the reaction. Protein was linked at a final reaction concentration of 1 or 5 μM, and the remaining active sites on protein-linked beads were blocked with 1 M Tris-HCl, pH 8.0, 100 mg/ml BSA; washed; and stored in assay buffer containing 50% glycerol.

Binding Assays—Binding assays were conducted as previously reported (8). Briefly, Arg- or Arg fragment-linked beads were added to binding reactions at a final concentration of 1 μM. For determination of the β1-Arg kinase domain binding interface, GST-β1 tails were added to binding reactions at a final concentration of 1 μM. For determination of K_d values, an increasing concentration gradient of GST-β1 from 0 to 5 μM was used. Reactions were performed for 1 h at 4 °C before washing and resuspending in Laemmli sample buffer (LSB).[7] Pull-down products were boiled and run on Bis-Tris PAGE gels, and gel bands were resolved with Coomassie Blue silver stain, and densities were quantified using QuantityOne software. For measurements of K_d, band densities were plotted against concentration of the free solution protein, and binding isotherms were set using GraphPad software using the one-site specific binding equation, $Y = B_{max}{}^{*}X/(K_d + X)$, where Y is specific binding, X is the concentration of the ligand, B_{max} is the maximum specific binding in the same units as Y, and K_d is the binding affinity in the same units as X.

In Vitro Kinase Assays—Nonradioactive *in vitro* kinase assays were performed using recombinant purified His-Arg and various GST-β1 tails. Arg was included in each reaction at a final concentration of 180 nM. Each GST-β1 tail was included at final concentrations ranging from 0.28 to 6.9 μM. The reactions were conducted in 25 mM Hepes, pH 7.25, 100 mM NaCl, 5% glycerol, 0.01% Triton X-100, 1 mM DTT, 5 mM $MgCl_2$, 5 mM $MnCl_2$, 20 ng/ml BSA, 1 mM sodium orthovanadate, and 50 μM ATP. After 2 h at 32 °C, reactions were quenched with 4× LSB and separated on 10% SDS-PAGE gels, transferred, immunoblotted with the 4G10 α-phosphotyrosine antibody, and then stripped and reprobed for GST using an α-GST antibody.

Radiolabeled *in vitro* kinase assays containing Arg and integrin β tails were performed as follows. Time-dependent kinase assays were performed by preincubating 50 nM Arg and 4 μM β tails in a buffer containing 25 mM Hepes, pH 7.25, 100 mM NaCl, 5% glycerol, 5 mM $MgCl_2$, 5 mM $MnCl_2$, 1 mM sodium pervanadate, 1 mM DTT for 5 min at 32 °C before spiking in 5 μM ATP with 0.75 μCi of [γ-^{32}P]ATP for 1–60 min before terminating with LSB, running on gels, and exposing to a phosphorimaging screen. Screens were scanned using a Personal Molecular Imager (Bio-Rad), and band densities were quantified using ImageJ software. For measuring the concentration dependence, the assays were performed as above except along a 14-point increasing β tail concentration series from 0.0625 to 4 μM. The reactions were performed for 60 min and analyzed as above. Radiolabeled β3 tail phosphorylation site mapping experiments were performed as above with 1 μM final concentration of tail in 60-min kinase reactions.

For *in vitro* Arg activation experiments, 0.1 nM purified recombinant His-Arg was preincubated with 62.5 nM GST or GST-β1 variants for 10 min at 32 °C in a buffer containing 25 mM Hepes, pH 7.25, 100 mM NaCl, 5% glycerol, 5 mM $MgCl_2$, 5 mM $MnCl_2$, 1 mM sodium pervanadate, 1 mM DTT, before the addition of GST-CrkII along a concentration gradient of 0.125–2 and 5 μM ATP with 0.75 μCi [γ-^{32}P]ATP for an additional 5 min at 32 °C. All reactions were quenched with LSB, boiled, and separated on 10% Bis-Tris PAGE gels. The gels were exposed to a phosphorimaging screen overnight and scanned using a Personal Molecular Imager (Bio-Rad) and quantified using ImageJ software. The values for each concentration series were fit to Michaelis-Menten isotherms, $Y = V_{max}{}^{*}X/(K_m + X)$, where Y is the enzyme velocity, V_{max} is the maximum enzyme velocity in the same units as Y, X is the substrate concentration, and K_m is the Michaelis-Menten constant in the same units as X. GraphPad software was used to obtain the K_m values for each condition. Gels were also stained with Blue Silver G-250 Coomassie for 30 min to visualize CrkII protein bands. Specific and

[7] The abbreviations used are: LSB, Laemmli sample buffer; SH, Src homology domain; pβ1, phosphorylated Tyr-783 β1; FLIM, fluorescence lifetime imaging microscopy; RFP, red fluorescent protein.

negative control bands were cut out and scintillation counted along with a 1-μl sample from the kinase assay. The number of counts per minute was calculated and correlated to integrated density from ImageJ software, and k_{cat} values were determined as previously (19).

Integrin β1 Phosphorylation and Arg Activation Assays in Cells—Phoenix cells were transiently transfected with WT or mutant Arg-RFP or Arg-YFP DNA using calcium phosphate or Lipofectamine 2000 (Invitrogen) transfection methods. 48 h after transfection, integrin receptors were activated by treatment with 2 mM Mn^{2+} (as $MnCl_2$) for 1 h. Some conditions were then treated with 5 μM STI-571 (or control DMSO) for an additional 2 h. Where stated, some experimental conditions included overnight pretreatment with 10 μM STI-571 or 30 μM DPH before Mn^{2+} activation. Cells were lysed in 25 mM Hepes, pH 7.25, 150 mM NaCl, 5% glycerol, 0.5% Nonidet P-40, 1 mM DTT, 0.5 mM sodium pervanadate, and protease inhibitors. Lysates were run on 8% Bis-Tris PAGE gels, transferred to nitrocellulose membranes, and blotted with either the integrin β1 Tyr(P)-783 specific antibody, or for integrin β1.

To assess the effects of integrin activation on Arg kinase activity in cells, WT or mutant Arg-RFP or Arg-YFP constructs were transiently transfected into Phoenix cells as described above. Cells were treated with or without Mn^{2+} for 1 h, and some conditions were further treated for 2 h with either 5 μM STI-571 or DMSO as above. Cells were lysed and run on Bis-Tris PAGE gels as above and transferred and blotted for phosphotyrosine or actin as a loading control. Tyrosine phosphorylation of proteins in the lysate was measured as the density of each lane using QuantityOne software. Relative levels of phosphorylation were normalized based on treatment times.

Phosphorylation of the Arg specific substrate cortactin was also measured from Phoenix or WT or $\beta1^{-/-}$ fibroblasts as above, except, where stated, some experimental conditions were pretreated overnight with 20 μM STI-571 prior to Mn^{2+} activation experiments. Following cell lysis, cortactin was immunoprecipitated using the 4F11 cortactin antibody, and immunoprecipitated products were run on Bis-Tris gels, transferred, and then blotted for phosphotyrosine. Blots were stripped and reprobed for cortactin, and inputs for each condition were run and blotted for proteins as indicated.

Immunoprecipitation Arg Kinase Assays—For immunoprecipitation kinase assays used to test the ability of Arg to phosphorylate GST-β1 tails, Arg-YFP was expressed in Phoenix cells for 48 h by the Lipofectamine transfection method before lysing in 25 mM Hepes, pH 7.25, 150 mM NaCl, 5% glycerol, 0.5% Nonidet P-40, 1 mM DTT, 1 mM sodium pervanadate, and protease inhibitors. Lysates were precleared with protein A/G-agarose beads (Pierce), and 100 μg of lysate was incubated for >3 h at 4 °C with an α-GFP antibody (Rockland) to immunoprecipitate Arg-YFP. Immunocomplexes were incubated with protein A/G-agarose beads for 1 h at 4 °C before spinning down, and beads were washed once with the above buffer containing 5 mM EDTA, two times with the above buffer, two times with assay buffer, and once with assay buffer containing 5 mM Mg^{2+} (as $MgCl_2$) and 5 mM Mn^{2+} (as $MnCl_2$). Arg immunocomplex bound beads were resuspended in 10 μl of assay buffer containing 5 mM Mg^{2+} (as $MgCl_2$) and 5 mM Mn^{2+} (as $MnCl_2$) and preincubated for 5 min at 32 °C with 10 μl of GST control or GST-β1 tail constructs at a final concentration of 2 μM. Following a 5-min preincubation, reactions were initiated through the addition of 5 μM ATP and 1 μCi of [γ-^{32}P]ATP for a 20-min kinase assay before quenching with LSB. The reactions were boiled, run on 8% Bis-Tris PAGE gels, exposed to a phosphorscreen overnight, and scanned and analyzed as described above.

For Arg activation assays in WT or $\beta1^{-/-}$ fibroblasts, cells were pretreated overnight with or without 20 μM STI-571 and then treated with or without 2 mM Mn^{2+} for 2 h before lysing as above in 25 mM Hepes, pH 7.25, 150 mM NaCl, 5% glycerol, 0.5% Nonidet P-40, 1 mM DTT, 1 mM sodium pervanadate, and protease inhibitors. Arg was immunoprecipitated using the monoclonal anti-Ar11 antibody (a gift from Peter Davies, Albert Einstein College of Medicine) for 5 h at 4 °C before incubation for 1 h at 4 °C with protein A/G-agarose beads. Beads were then washed as above. Arg immunocomplex bound beads were resuspended in 10 μl of assay buffer containing 5 mM Mg^{2+} (as $MgCl_2$) and 5 mM Mn^{2+} (as $MnCl_2$) and preincubated for 5 min at 32 °C with 10 μl of recombinant purified GST-CrkII in assay buffer at a final concentration of 1 μM. Following the preincubation period, reactions were initiated through addition of 5 μM ATP and 1 μCi of [γ-^{32}P]ATP for a 5-min kinase assay before quenching with LSB. Reactions were boiled, run on 8% Bis-Tris PAGE gels, exposed to a phosphorscreen overnight, and scanned and analyzed as described above.

Measurement of Arg SH2 Domain Binding to Phosphorylated Integrin β1—The GST-Arg-SH3-SH2 or GST-Arg-SH2 domains were purified from bacteria and linked to beads as described above. GST-β1 tails were phosphorylated with Arg as described above, washed with high salt to remove Arg, and then buffer-exchanged into assay buffer for use in binding assays. Phosphorylation was confirmed by immunoblotting the repurified GST-tagged proteins with the 4G10 anti-phosphotyrosine antibody. Binding assays were then performed with Arg-SH3-SH2 or Arg-SH2 domain-linked beads as described above.

FLIM-based FRET Measurements—Experiments were performed, and FRET efficiencies were analyzed as described previously (17). Briefly, cells were transfected with a 1:1.5 or 1:2 ratio of GFP:mCherry/RFP (donor:acceptor) plasmids and allowed to express for 36 h. Cells were fixed in 4% paraformaldehyde and permeabilized in 0.2% (w/v) Triton X-100 in PBS. After quenching with 1 mg/ml sodium borohydride in PBS for 10 min at room temperature, the cells were washed in PBS and mounted in Mowiol containing 2.5% Dabco (Sigma-Aldrich). Time domain FLIM was performed with a multiphoton microscope system (with TE2000 microscope; Nikon) described in detail previously (17). Fluorescence lifetime imaging capability was provided by time-correlated single-photon counting electronics (SPC-700; Becker and Hickl). A 40× objective was used throughout (Plan Fluor NA 1.3; CFI 60; Nikon), and data were collected at 500 ± 20 nm through a band pass filter (catalog no. 35-5040; Coherent, Inc.). Only cells expressing 1:1 ratio or above of donor:acceptor molecules were used for imaging throughout to ensure acceptor levels were nonlimiting. Acquisition times of the order of 300 s at a low 890-nm excitation power were used to achieve sufficient photon statistics for fitting, while avoiding either pulse pile up or significant photo-

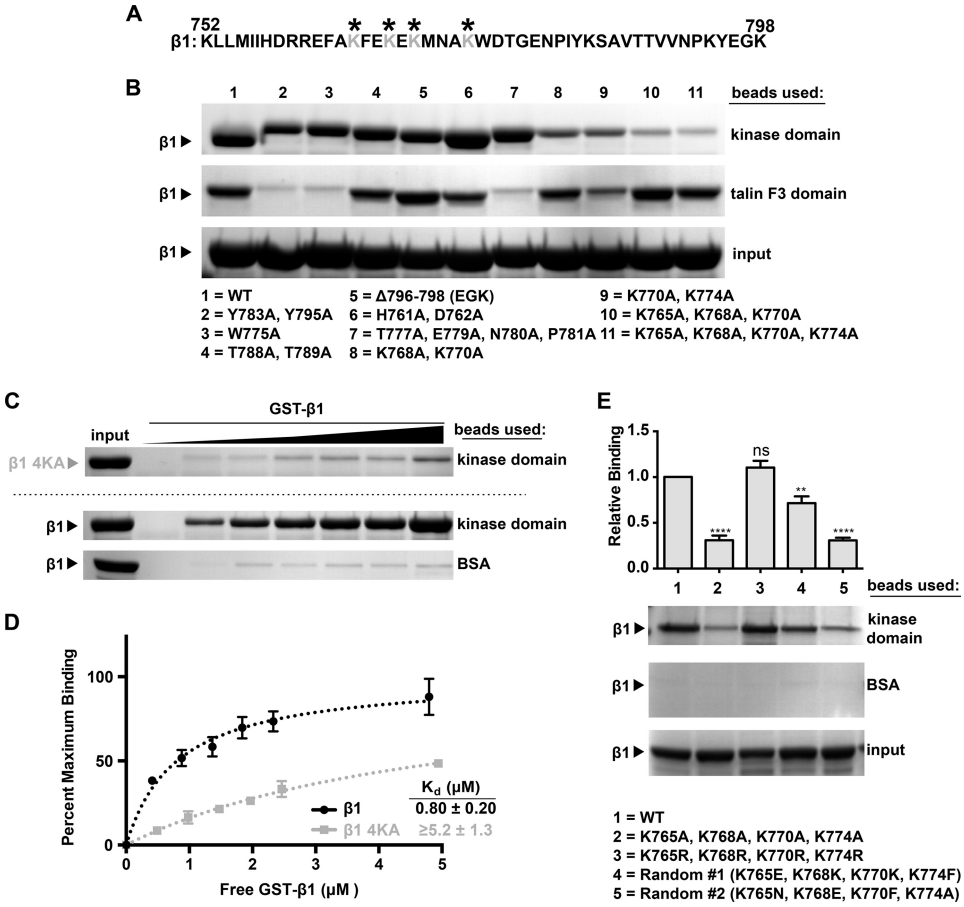

FIGURE 1. **The Arg kinase domain binds to a lysine-rich region in the integrin β1 tail.** *A*, amino acid sequence of the 47-residue integrin β1A cytoplasmic tail. The lysine residues that mediate interactions with Arg are indicated by *asterisks*. *B*, binding of Arg kinase domain to various integrin β1A cytoplasmic tail mutants. Agarose beads were coupled to Arg kinase domain (*top panel*) or the talin F3 domain (*middle panel*), incubated with GST-β1 tail or GST-β1 tail mutants, and washed, and bound material was analyzed on Bis-Tris PAGE gels and Coomassie Blue-stained. Mutations to the talin F3 domain binding interface (*lanes 2*, *3*, and *7*) abrogate talin F3 binding but do not affect Arg kinase domain binding. Similarly, mutations in the known Src nonreceptor tyrosine kinase interface, Δ796–798 (*lane 5*), and the kindlin-1/kindlin-2 interface, T788A/T789A (*lane 4*), do not affect Arg kinase binding. However, mutation of four lysine residues in the membrane-proximal half of the tail significantly reduces Arg kinase domain binding (*lane 11*). *C*, the concentration dependence of GST-β1 and GST-β1–4KA (K765A/K768A/K770A/K774A) binding to Arg kinase domain was measured. *D*, one-site specific binding isotherms fit using GraphPad software were set to binding experiments in *C*. The K_d value for the GST-β1-Arg kinase domain is 0.80 ± 0.20 μM. Saturated binding of Arg kinase domain binding to GST-β1–4KA could not be achieved, and thus we could only place a lower limit of affinity for this interaction of $K_d \geq 5.2$ μM. *Error bars* represent the S.E. from $n = 3$ for each condition. *E*, requirements of β1 tail amino acid charge and position for binding the Arg kinase domain. Beads were linked as before with Arg kinase domain or control BSA and incubated in binding assays with WT GST-β1 or GST-β1–4KA, GST-4KR, or two tails in which the 10 amino acids between Lys-765 and Lys-774 were randomized (GST-β1-Random #1 and -Random #2). The 4KR mutant binds at WT levels, whereas both randomized sequences are binding-deficient, indicating that the β1 tail requires positively charged amino acids at positions 765, 768, 770, and 774 for optimal binding to the Arg kinase domain. *Error bars* represent S.E. from $n = 4$. *, $p < 0.05$; **, $p < 0.01$; ***, $p < 0.001$; *ns*, not significant compared with the WT condition.

bleaching. The data are plotted as mean FRET efficiency pooled from specified numbers of cells per sample over two or three independent experiments. Analysis of variance was used to test statistical significance between different populations of data. Lifetime images of example cells are presented using a pseudocolor scale, where blue depicts normal GFP lifetime (no FRET), and red depicts lower GFP lifetime (areas of FRET).

Statistical Analysis—Unless otherwise stated, Student's *t* tests (unpaired, two-tailed) were used to test for significance between conditions. For all experiments, $p < 0.05$ was considered significant. In some cases, no significant difference was explicitly stated by *ns* (not significant). Graphs are presented as means ± S.E.

RESULTS

A Lysine-rich Region in the Integrin β1 Cytoplasmic Tail Binds to the Arg Kinase Domain—Full-length Arg and the Arg kinase domain alone bind with micromolar affinity to a GST-integrin β1A cytoplasmic tail fusion protein (GST-β1), but the integrin β1 residues that comprise the Arg kinase domain binding site are unknown (8). We mutated residues in GST-β1 (Fig. 1*A*) that mediate interactions with known integrin β1 binding partners. For example, the Y783A/Y795A, W775A, and membrane-proximal NP*X*Y motif (N780A/P781A) mutations prevent talin binding (20–23), the T788A/T789A mutation prevents kindlin-1 and kindlin-2 binding to the β1 tail (24), and removal of the last three residues (Δ796–798) prevents Src family kinase binding to β tails (25, 26). We incubated these mutant GST-β1 tails with agarose beads covalently coupled to the Arg kinase domain. Each of these GST-β1 mutants was retained on Arg kinase domain beads at levels similar to WT GST-β1 (Fig. 1*B*). In contrast, although WT GST-β1 binds the talin F3 domain, the known talin binding-deficient mutations drastically reduced GST-β1 binding to the talin F3 domain (Fig. 1*B*, compare *lane 1* with *lanes 2*, *3*, and *7*). These data strongly

suggest that Arg and talin interact with the β1 tail via distinct residues.

We performed alanine-scanning mutagenesis of many of the other 47 amino acids in the β1 integrin tail (Fig. 1*A*). Initial analyses of point mutants revealed that mutation of individual lysine residues in the middle of the tail reduced, but did not eliminate, GST-β1 binding to the Arg kinase domain (data not shown). Subsequently, we found that mutating several of these

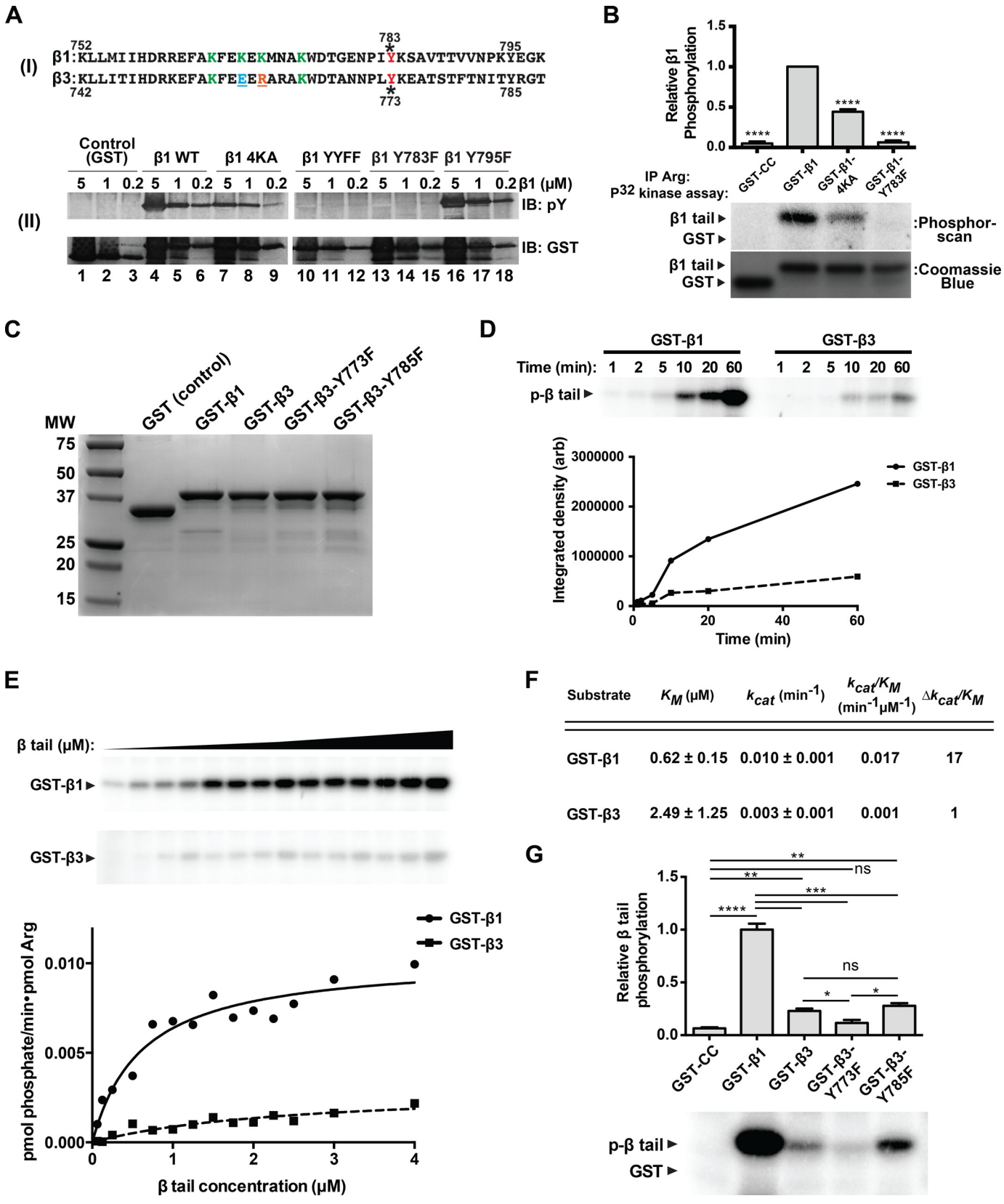

Substrate	K_M (μM)	k_{cat} (min^{-1})	k_{cat}/K_M ($min^{-1}\mu M^{-1}$)	$\Delta k_{cat}/K_M$
GST-β1	0.62 ± 0.15	0.010 ± 0.001	0.017	17
GST-β3	2.49 ± 1.25	0.003 ± 0.001	0.001	1

lysine residues (marked with *asterisks* in Fig. 1*A*) in tandem further reduced binding of GST-β1 to Arg kinase domain-coupled beads (Fig. 1*B*, compare *lane 1* with *lanes 8–10*). We therefore constructed a mutant bearing mutations in all four lysine residues (K765A/K768A/K770A/K774A, henceforth termed 4KA). GST-β1–4KA did not bind efficiently to Arg kinase domain beads (Fig. 1*B*, *lane 11*). We could not achieve concentrations of GST-β1–4KA high enough to achieve saturated binding, and thus we could only place a lower limit of $K_d \geq 5.2\ \mu$M to this interaction, as compared with $0.80 \pm 0.20\ \mu$M for GST-β1, a reduction of at least 6.5-fold in affinity (Fig. 1, *C* and *D*). Importantly, GST-β1–4KA binds the talin F3 fragment at levels comparable with WT GST-β1 (Fig. 1*B*, compare *lanes 1* and *11*), indicating that the 4KA mutations specifically disrupt binding to the Arg kinase domain and that reduced Arg binding does not result from global disruption of β1 tail structure. It initially appeared that the talin F3 domain bound less of the GST-β1-K770A, K774A mutant relative to WT GST-β1 (Fig. 1*B*, *lane 9*, in the *talin F3 domain panel*). We subsequently monitored the concentration dependence of this interaction and observed similar binding affinities between talin F3 and WT GST-β1 or GST-β1-K770A, K774A ($K_d = 0.56 \pm 0.10\ \mu$M for WT GST-β1 and $K_d = 0.31 \pm 0.02\ \mu$M for GST-β1-K770A, K774A; data not shown). Together, these findings suggest that talin F3 and Arg kinase may engage nonoverlapping residues in the β1 tail. We also noted that only lysines 765 and 774 are conserved in integrin β3 (Fig. 2*A*), which may explain the greatly reduced binding of the Arg kinase domain for a similar GST-β3 tail fusion protein (8).

To further explore whether positively charged residues at positions 765, 768, 770, and 774 were necessary in mediating the Arg kinase domain-β1 binding event, we measured Arg kinase domain binding to a GST-β1 tail mutant bearing mutations of the four lysines to arginines (K765R, K768R, K770R, and K774R). The Arg kinase domain bound to this GST-β1–4KR mutant similarly to WT GST-β1, revealing that the Arg kinase domain-β1 tail interaction requires positively charged residues at these positions (Fig. 1*E*, compare *lanes 1–3*). We also tested whether the position of the lysines, which are believed to emerge from the same side of a helical structure (23), was an important determinant of the integrin β1 tail-Arg kinase domain interaction. We randomized the 10 amino acids in GST-β1 from Lys-765 to Lys-774 while maintaining their overall amino acid composition to create two distinct mutants: Random #1 and Random #2 (Fig. 1*E*). GST-β1-Random #1 retained lysines in positions 768 and 770, and its relative ability to bind the Arg kinase domain was intermediate between that of WT GST-β1 and GST-β1–4KA (Fig. 1*E*, *lane 4*). GST-β1-Random #2 did not retain lysines at any of the positions of WT GST-β1, and it bound the Arg kinase domain at greatly reduced

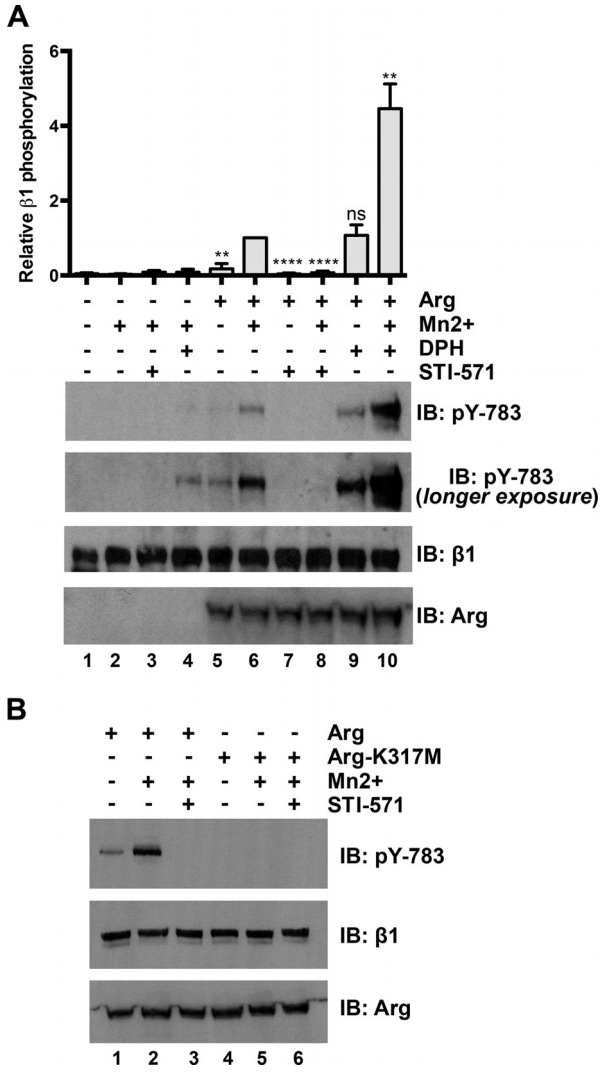

FIGURE 3. **Arg phosphorylates Tyr-783 on integrin β1 in cells.** *A*, Arg phosphorylates endogenous integrin β1 at site Tyr-783 in cells. Control or Arg-YFP-expressing Phoenix cells were pretreated overnight with STI-571 (10 μM) or DPH (30 μM) before performing Mn^{2+}-mediated integrin activation assays where some conditions were treated with 2 mM Mn^{2+} to activate integrins. STI-571 suppresses and DPH enhances Mn^{2+}-activated integrin Tyr-783 phosphorylation in Arg-YFP-expressing Phoenix cells. *Error bars* represent S.E. from $n = 3$. **, $p < 0.01$; ****, $p < 0.0001$; *ns*, not significant relative to the integrin-activated Arg-YFP condition (*lane 6*). *B*, Arg-YFP or kinase inactive Arg-K317M-YFP were expressed in Phoenix cells, and Mn^{2+}-stimulated integrin activation assays were performed as above before blotting Tyr(P)-783. An Arg kinase inactive mutant (K317M) cannot promote Tyr-783 phosphorylation in cells. *IB*, immunoblot.

FIGURE 2. **Arg phosphorylates integrin β1 at Tyr-783.** *A*, *panel (I)*, sequence comparison between β1 and β3 tails. *Panel (II)*, kinase assays were performed using Arg and GST, GST-β1, GST-β1–4KA, GST-β1-YYFF, GST-β1-Y783F, or GST-β1-Y795F as substrates. Reactions were run on SDS-PAGE gels and immunoblotted (*IB*) with anti-phosphotyrosine or anti-GST antibodies. No phosphorylation of either GST-β1-YYFF or GST-β1-Y783F was detected, indicating that Tyr-783 is required for Arg-mediated GST-β1 phosphorylation. *B*, Arg-YFP was expressed and immunoprecipitated (*IP*) from Phoenix cells and used in radiolabeled kinase assays with GST (control) or GST-β1 tails. Immunoprecipitated Arg-YFP does not phosphorylate the Y783F mutant and exhibits a significantly diminished ability to phosphorylate the 4KA mutant. *Error bars* represent S.E. from $n = 3$ for each condition. ****, $p < 0.0001$ compared with the GST-β1 condition. *C*, Coomassie Blue-stained gel image showing purity of WT or mutant GST-β1 and -β3 tail constructs used in experiments shown in the remainder of the figure. *MW*, molecular weight. *D*, time-dependent radiolabeled kinase assays measuring the ability of Arg to phosphorylate the GST-β1 or -β3 tails. *E*, radiolabeled kinase assays measuring the activity of Arg on increasing concentrations of GST-β1 or -β3 tails. *F*, data from *E* were fit to the Michaelis-Menten equation in GraphPad to obtain kinetic parameters. Arg exhibits a 17-fold enhancement in catalytic efficiency for GST-β1 compared with GST-β3. *G*, β3 tail phosphorylation site identification. Radiolabeled kinase assays were performed with GST control, GST-β1, or WT or single phosphorylation site mutant GST-β3 tails. Arg preferentially phosphorylates the membrane-proximal site in the β3 tail. *Error bars* represent S.E. from $n = 3$ for each condition. *, $p < 0.05$; **, $p < 0.01$; ***, $p < 0.001$; *ns*, not significant.

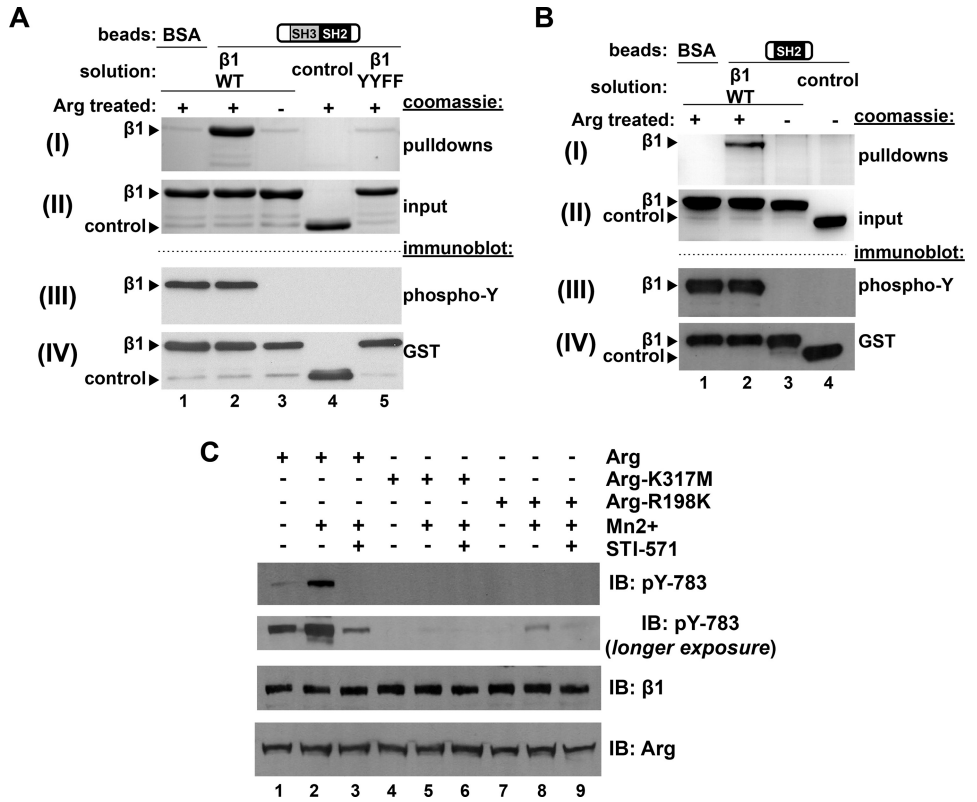

FIGURE 4. **Arg-mediated Tyr-783 phosphorylation introduces a second binding interface for the Arg SH2 domain and is required for further Tyr-783 phosphorylation.** *A*, beads covalently linked to the Arg-SH3-SH2 fragment or BSA were incubated with either Arg prephosphorylated GST-β1 (GST-pβ1), nonphosphorylated GST-β1, GST (control), or nonphosphorylatable GST-β1-YYFF, and bound material was run on gels and Coomassie Blue-stained. *Panel (I)* is a Coomassie Blue-stained gel image of the pulldown product. Arg-SH3-SH2 but not BSA linked beads pulled down GST-pβ1 (compare *lanes 1* and *2*) but not GST-β1, GST, or GST-β1-YYFF (compare *lane 2* with *lanes 3–5*). *Panel (II)* is a Coomassie Blue-stained gel showing 5% of the total input protein in each binding reaction. *Panel (III)* is an anti-phosphotyrosine immunoblot (*IB*), and *panel (IV)* is an anti-GST immunoblot of GST-β1 tails. *B*, beads covalently coupled to the Arg-SH2 domain alone were tested for binding GST-β1 variants, as outlined in *A*. Arg-SH2 domain linked beads pulled down GST-pβ1 but not GST-β1 or GST (control), indicating this interaction is mediated by the Arg SH2 domain. *C*, the Arg SH2 domain is required for efficient Tyr-783 phosphorylation in cells. Phoenix cells were transfected with Arg-YFP, kinase inactive Arg-K317M-YFP, or SH2 interaction abrogating mutant Arg-R198K-YFP, and Mn^{2+} integrin activation assays were performed. Arg-R198K produced intermediate levels of Tyr(P)-783 relative to Arg and Arg-K317M.

levels, similar to the reduced levels observed with GST-β1–4KA-Arg kinase domain binding (Fig. 1*E*, *lane 5*). Together, these data indicate that positively charged amino acids at positions 765, 768, 770, and 774 positions of the β1 tail are critical for high affinity binding to the Arg kinase domain.

Arg Phosphorylates β1 at the Membrane-proximal Tyrosine Residue—Two tyrosine residues, Tyr-783 and Tyr-795, each part of N*XX*Y motifs in the β1 tail, mediate interactions with talin and kindlin family proteins, respectively, and phosphorylation of these sites disrupts binding by their respective partners (27–29). We asked whether Arg, by virtue of its ability to bind integrin β1, could phosphorylate either of these residues. GST-β1 was phosphorylated by purified recombinant Arg *in vitro*, but a GST-β1 mutant with tyrosine to phenylalanine substitutions at both residues (GST-β1-YYFF) was not, indicating that Arg phosphorylates one or both of the tyrosines in the β1 tail (Fig. 2*A*). Mutation of Tyr-783 (Y783F) abrogated β1 phosphorylation, whereas mutation of Tyr-795 (Y795F) did not affect β1 phosphorylation (Fig. 2*A*). These data indicate that Arg phosphorylates the integrin β1 tail specifically on Tyr-783. Importantly, the phosphorylation of the GST-β1–4KA mutant was reduced for each concentration tested, consistent with the significantly reduced affinity this mutant has for the Arg kinase domain (Fig. 2*A*). Further, Arg-YFP immunoprecipitated from HEK 293T-derived Phoenix cells did not phosphorylate the integrin β1 tail Y783F mutant and exhibited a significantly reduced ability to phosphorylate the Arg kinase domain interaction deficient integrin β1 tail (4KA), indicating that kinase domain engagement potentiates phosphorylation of β1 at site Tyr-783 by Arg (Fig. 2*B*).

Arg exhibits reduced affinity for the integrin β3 tail relative to the integrin β1 tail (8). We therefore tested whether Arg phosphorylates the GST-β1 tail preferentially over the GST-β3 tail. Using time-dependent radiolabeled kinase assays, we found that Arg displayed a clear preference in phosphorylating the GST-β1 tail *versus* the GST-β3 tail (Fig. 2, *C* and *D*). Measurement of the K_m and k_{cat} values for Arg-mediated phosphorylation revealed that Arg strongly prefers β1 as a substrate, exhibiting a 17-fold greater catalytic efficiency (k_{cat}/K_m) for GST-β1 compared with GST-β3 (Fig. 2, *E* and *F*). Using GST-β3 Y773F and Y785F tail mutants as substrates, we found that the Y773F mutation eliminates most of the Arg-mediated GST-β3 phosphorylation, indicating that Arg preferentially phosphorylates GST-β3 on Tyr-773 (Fig. 2*G*).

Finally, we tested whether Arg could phosphorylate integrin β1 in cells. To test whether Arg activity is required for phosphorylation of endogenous integrin β1 at site Tyr-783, we pretreated control or Arg-expressing Phoenix cells with STI-571

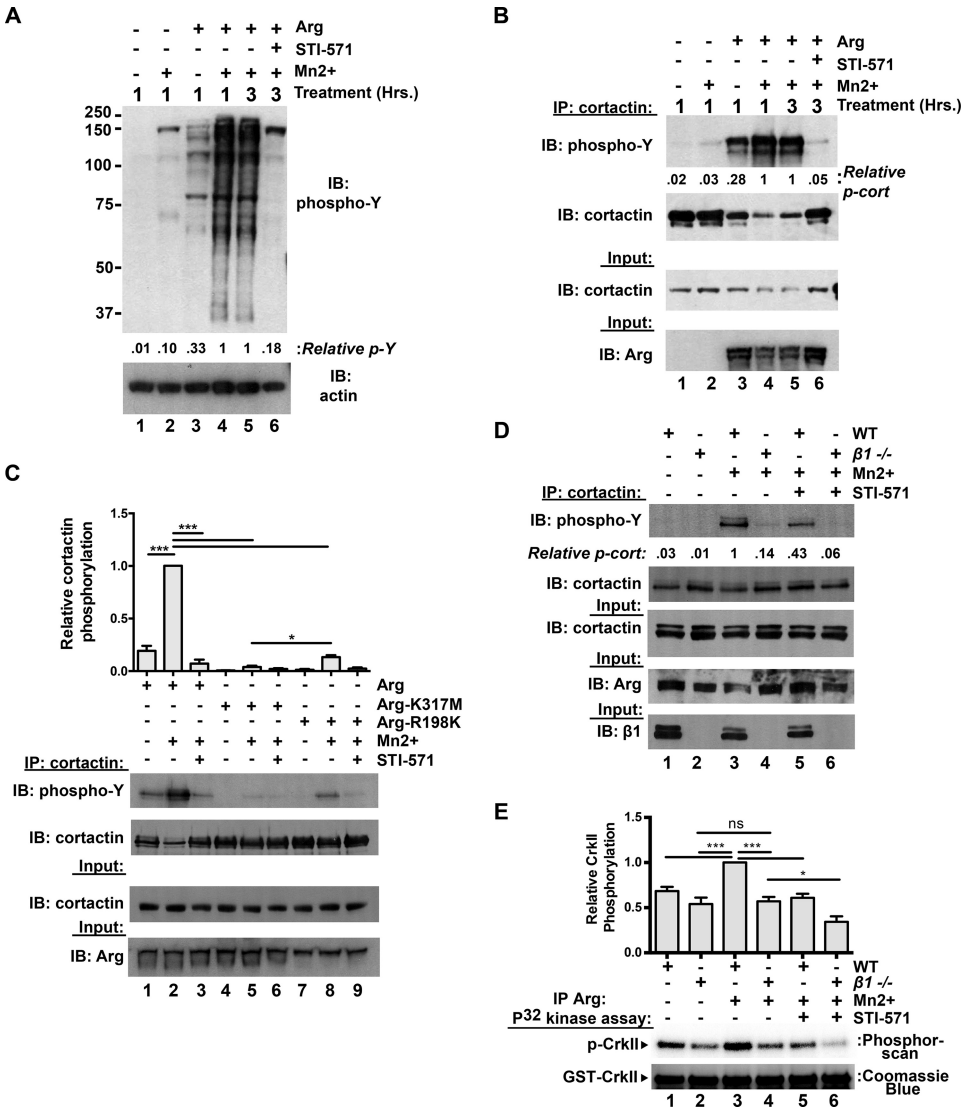

FIGURE 5. **Integrin activation potentiates Arg kinase activation in cells.** *A*, integrin activation enhances Arg-dependent global protein phosphorylation in cells. Control or Arg-RFP-expressing Phoenix cells were treated with or without Mn^{2+} for 1 h to activate integrins. Some conditions were then lysed (*lanes 1–4*), whereas other conditions (*lanes 5* and *6*) were further treated with 5 μM STI-571 or DMSO vehicle control for an additional 2 h (3 h of total Mn^{2+} treatment) before cell lysis. Lysates were then separated on Bis-Tris PAGE gels and immunoblotted (*IB*) for phosphotyrosine. Integrin activation strongly enhances Arg-mediated phosphorylation of proteins in the lysate (compare *lanes 3* and *4*), but co-treatment of integrin activated Arg-RFP-expressing cells with 5 μM STI-571 (compared with DMSO vehicle control) attenuates this phosphorylation (compare *lanes 5* and *6*). *B*, integrin activation drives Arg-mediated cortactin phosphorylation. Control or Arg-RFP-expressing Phoenix cells were treated as in *A*, cortactin was immunoprecipitated (*IP*) from cell lysates and immunoblotted with anti-phosphotyrosine antibodies. Integrin activation results in elevated cortactin phosphorylation in Arg-RFP-expressing cells (compare *lanes 3* and *4*), which is attenuated by STI-571 treatment (compare *lanes 5* and *6*). *C*, the Arg SH2 domain is required for optimal integrin activation-mediated Arg kinase activation. Arg-YFP, kinase inactive Arg-K317M-YFP, and SH2 mutant Arg-R198K-YFP were expressed in Phoenix cells, and integrin activation assays were performed as in *B*. Arg-R198K-expressing cells exhibited intermediate levels of Arg-mediated cortactin phosphorylation, compared with WT and kinase inactive Arg-K317M-expressing cell conditions. *Error bars* represent S.E. from $n = 3$ for each condition. *, $p < 0.05$; ***, $p < 0.001$. *D*, integrin β1 activation drives Arg kinase activation. Isogenic WT or *integrin* $\beta1^{-/-}$ 3T3 fibroblast lines were treated with or without 2 mM Mn^{2+} for 2 h before lysing and immunoprecipitating cortactin. Immunoprecipitated products were then run on Bis-Tris gels, transferred, and immunoblotted for phosphotyrosine. Phosphorylated cortactin levels are markedly lower in *integrin* $\beta1^{-/-}$ 3T3 cells compared with WT, and Mn^{2+} induces a robust increase in phosphorylated cortactin in WT but not *integrin* $\beta1^{-/-}$ 3T3 cells. Image shown is representative of >3 independent experiments. *E*, Arg was immunoprecipitated from WT and *integrin* $\beta1^{-/-}$ 3T3 cells following treatments as performed in *D*, and its relative activity was measured in *in vitro* kinase assays using CrkII as a substrate. Mn^{2+}-mediated integrin activation enhances Arg activity in WT, but not *integrin* $\beta1^{-/-}$ cells. Overnight STI-571 (20 μM) pretreatment dampens Arg activity via both readouts described in *D* and *E*. *Error bars* represent S.E. from $n = 4$. *, $p < 0.05$; ***, $p < 0.001$; *ns*, not significant.

or the Abl family kinase activator DPH (30) before activating integrins with Mn^{2+}. The combination of DPH pretreatment and Mn^{2+} stimulation yielded an increase in integrin β1 Tyr-783 phosphorylation even in untransfected Phoenix cells (Fig. 3*A*, *panel (II)*, *lane 4*, longer exposure), indicating that endogenous Abl family kinases can phosphorylate integrin β1 following Mn^{2+} stimulation. In Phoenix cells that moderately expressed Arg-YFP, STI-571 pretreatment diminished both basal and Mn^{2+}-stimulated Tyr-783 phosphorylation (Fig. 3*A*, compare *lanes 5–8*), whereas DPH pretreatment enhanced Tyr-783 phosphorylation 4–5-fold over that of basal and Mn^{2+}-stimulated levels (Fig. 3*A*, compare *lanes 5*, *6*, *9*, and *10*). Finally, an Arg kinase inactive point mutant (Arg-K317M) (5, 16) did not promote Tyr-783 phosphorylation of endogenous

integrin β1 following Mn^{2+} stimulation (Fig. 3*B*). Together, these data demonstrate that integrin activation triggers Arg-mediated phosphorylation of integrin β1 at Tyr-783 in cells.

The Arg SH2 Domain Binds the Phosphorylated β1 Integrin Tail—Abl family kinases are held in an inactive conformation through intramolecular interactions between the kinase domain and the adjacent SH2 and SH3 domains (31–33). Ligands such as Rin1 interact with the SH3 and SH2 domains and shift the equilibrium of the kinase into the active conformation (34). We hypothesized that tyrosine-phosphorylated β1 could similarly serve as a binding site for the Arg SH2 domain. Following *in vitro* phosphorylation of the GST-β1 tail (Fig. 4*A*, *panel (III)*), we measured the ability of phosphorylated (pβ1) or nonphosphorylated β1 to bind to an Arg fragment containing its SH3 and SH2 domains covalently linked to agarose beads (14). The Arg-SH3-SH2 domain-coupled beads bound phosphorylated β1, but not nonphosphorylated β1 (Fig. 4*A*, *panel (I)*, compare *lanes 2* and *3*). Neither control GST nor the GST-β1-YYFF integrin mutants were phosphorylated by Arg *in vitro* (Fig. 4*A*, *panel (III)*, *lanes 4* and *5*), and these proteins did not bind Arg-SH3-SH2-coupled beads (Fig. 4*A*, *panel (I)*, *lanes 4* and *5*). Similar experiments performed with beads coupled to the isolated Arg SH2 domain revealed that it was sufficient to bind the pβ1 tail (Fig. 4*B*). These experiments demonstrate that the Arg-SH2 domain binds specifically to the phosphorylated β1 tail.

The Arg SH2 Domain Is Required for β1 Phosphorylation in Cells—We hypothesized that the Arg SH2 domain-Tyr(P)-783-β1 interaction may promote integrin β1 phosphorylation in cells, by adding an additional anchoring interface at the membrane. To test this hypothesis, we performed Mn^{2+}-mediated integrin activation assays in Phoenix cells expressing Arg R198K, which bears a point mutant that disrupts its SH2 domain binding to phosphotyrosine motifs (5). Following Mn^{2+} treatment, we observed greatly reduced levels of integrin β1 Tyr-783 phosphorylation in Arg R198K-expressing cells compared with control cells expressing WT Arg (Fig. 4*C*, compare *lanes 2* and *8*). This level of integrin β1 phosphorylation was consistently higher than in cells bearing the Arg kinase inactive mutant (Arg-K317M) (5, 16) (Fig. 4*C*, compare *lanes 5* and *8*). Using immunoprecipitation kinase assays, we verified that Arg R198K had kinase activity that was similar to WT Arg *in vitro* (data not shown). These experiments indicate that a functional Arg SH2 domain is required to promote efficient integrin β1 Tyr-783 phosphorylation in cells.

Integrin β1 Binding Activates Arg Kinase Activity—Having defined two distinct interaction interfaces between integrin β1 and Arg, we next tested how these interactions influenced Arg kinase activity. We first tested how integrin activation affects activation of Arg following modest overexpression in Phoenix cells. Mn^{2+}-stimulated integrin activation in Arg-RFP-expressing cells led to a global increase in phosphorylated proteins as assayed by an anti-phosphotyrosine immunoblot of the lysate (Fig. 5*A*, compare *lanes 3* and *4*). Further, treatment of integrin-activated Arg-RFP-expressing cells with STI-571 attenuated this increased global cellular phosphorylation (Fig. 5*A*, compare *lanes 5* and *6*). We next measured phosphorylation of the Arg substrate cortactin (5, 16) following integrin activation

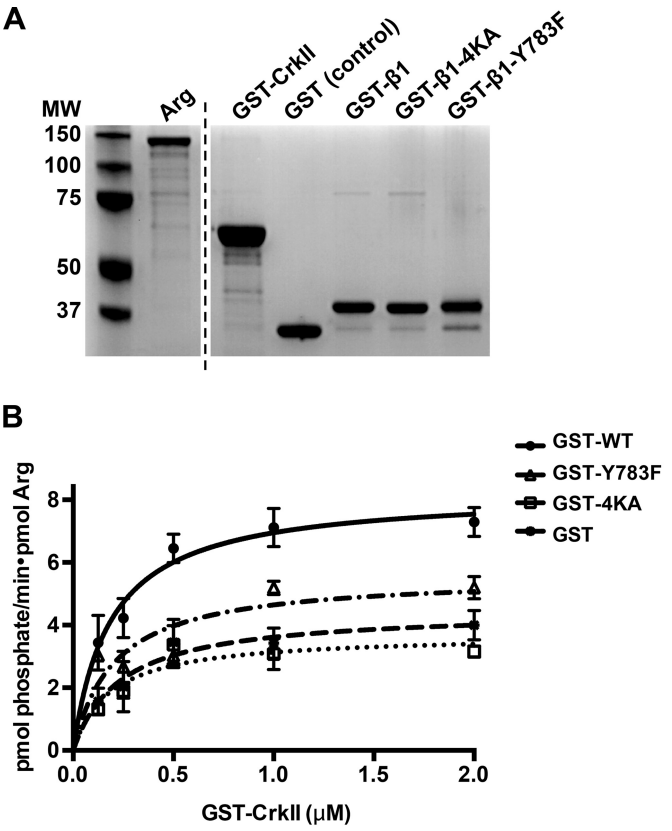

C

Substrate	Preincubation Construct	K_M (μM)	k_{cat} (min^{-1})	k_{cat}/K_M ($min^{-1}μM^{-1}$)	$\Delta k_{cat}/K_M$
GST-CrkII	GST-β1	0.19 ± 0.06	8.24 ± 0.67	44.25	2.34
GST-CrkII	GST-β1 Y783F	0.20 ± 0.08	5.59 ± 0.59	27.49	1.46
GST-CrkII	GST-β1 4KA	0.18 ± 0.08	3.70 ± 0.44	20.34	1.08
GST-CrkII	GST (Control)	0.24 ± 0.13	4.47 ± 0.71	18.87	1.00

FIGURE 6. **Direct interactions with integrin β1 modulate Arg kinase activation *in vitro*.** *A*, Coomassie Blue-stained gel showing the purity of all recombinant purified proteins used in this figure. The *vertical dashed line* separates nonconsecutive regions of proteins resolved on the same gel. *MW*, molecular weight. *B*, 0.1 nM Arg was preincubated with 62.5 nM GST (control), or GST-β1 tails, or Arg interaction deficient mutants thereof, and kinase activity was assayed by determining the kinetic parameters of GST-CrkII phosphorylation in [γ-^{32}P]ATP kinase assays. Measurements collected along an increasing concentration gradient of CrkII in each condition were fit to Michaelis-Menten isotherms using GraphPad software. *Error bars* represent the S.E. from $n \geq 3$ concentration series for each condition. *C*, K_m, k_{cat}, and the catalytic efficiency (k_{cat}/K_m) values of Arg-mediated GST-CrkII phosphorylation were calculated from isotherms fit to respective Arg kinase assays shown in *B*. Arg preincubation with GST-β1 leads to a 2.34-fold enhancement in catalytic efficiency compared with the GST control.

using the same experimental setup. As with β1 phosphorylation, cortactin phosphorylation was greatly increased in Arg-RFP-expressing cells upon integrin activation, and this was diminished upon treatment with STI-571 (Fig. 5*B*). We noted that total soluble cortactin levels in the cell lysate were reduced in the integrin-activated Arg-RFP-expressing cells (Fig. 5*B*, *lanes 4* and *5*). This cortactin insolubility has previously been

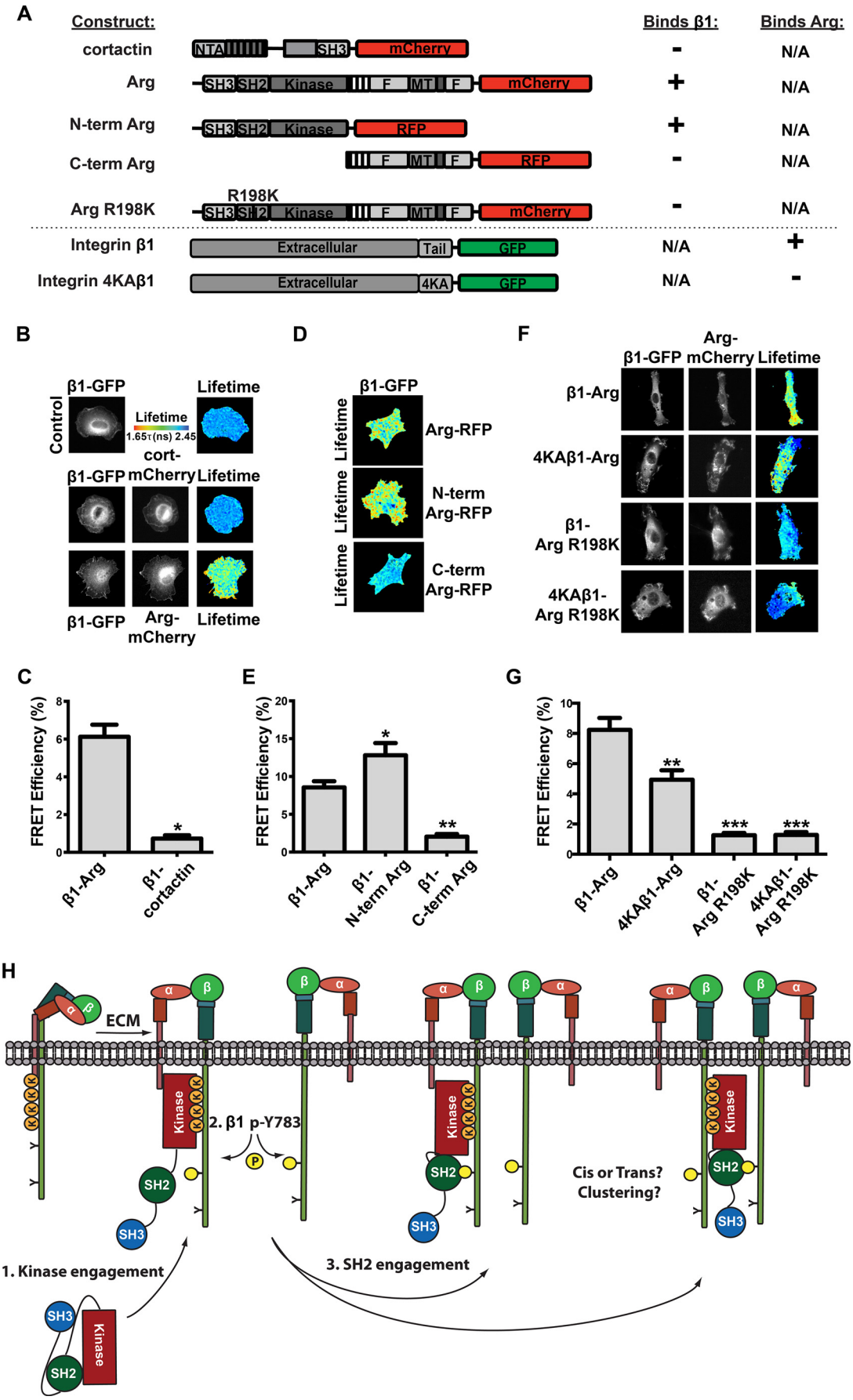
A
Construct:
Binds β1:
Binds Arg:
cortactin
NTA
SH3
mCherry
Arg
SH3 SH2 Kinase F MT F
N-term Arg
RFP
C-term Arg
Arg R198K
R198K
Integrin β1
Extracellular
Tail
GFP
Integrin 4KAβ1
4KA
B
β1-GFP
Lifetime
Control
Lifetime
1.65τ(ns) 2.45
cort-
mCherry
Arg-
D
Arg-RFP
N-term Arg-RFP
C-term Arg-RFP
F
β1-Arg
4KAβ1-Arg
β1-Arg R198K
4KAβ1-Arg R198K
C
FRET Efficiency (%)
β1-Arg
β1-cortactin
E
β1-N-term Arg
β1-C-term Arg
G
4KAβ1-Arg
β1-Arg R198K
4KAβ1-Arg R198K
H
ECM
2. β1 p-Y783
Cis or Trans?
Clustering?
1. Kinase engagement
3. SH2 engagement

attributed to movement of phosphorylated cortactin into an insoluble, cytoskeleton-rich fraction (35–37). Further, we detected very little cortactin phosphorylation following integrin activation in cells expressing the kinase inactive Arg (Arg-K317M) mutant (Fig. 5*C*, compare *lanes 1–3* with *lanes 4–6*). Interestingly, we found that the Arg SH2 mutant R198K supports levels of cortactin phosphorylation that are intermediate between WT Arg and Arg-K317M (Fig. 5*C*, *lanes 7–9*). These data strongly suggest that Arg-mediated cortactin phosphorylation can be driven by integrin activation in cells.

Finally, we evaluated the requirement for integrin β1 in the regulation of cortactin phosphorylation in mouse 3T3 fibroblast lines. Following Mn^{2+} treatment, we observed a robust increase in cortactin phosphorylation in WT, but not isogenic $\beta1^{-/-}$ 3T3 cells (Fig. 5*D*, compare *lanes 1* and *2* with *lanes 3* and *4*). STI-571 pretreatment dampened global cortactin phosphorylation by 55–60%, suggesting that this proportion of Mn^{2+}-activated cortactin phosphorylation requires Abl family kinase activity (Fig. 5*D*, compare *lanes 3* and *4* with *lanes 5* and *6*). We also immunoprecipitated Arg from lysates of cells that had undergone these treatments and measured the ability of the immunoprecipitated Arg to phosphorylate its substrate CrkII *in vitro*. Mn^{2+} treatment led to a ~1.5-fold increase in Arg activity as read out by CrkII phosphorylation following integrin activation in WT 3T3 cells, but this activation was prevented by STI-571 treatment (Fig. 5*E*, *lanes 1*, *3*, and *5*). Importantly, Mn^{2+} treatment did not promote increased Arg kinase activity in $\beta1^{-/-}$ 3T3 cells (Fig. 5*E*, compare *lanes 2* and *4*), indicating that Mn^{2+} treatment acts through integrin β1 to promote Arg kinase activation in cells.

We next used *in vitro* kinase assays to test the role of specific β1-Arg interaction interfaces in Arg kinase activation. We incubated Arg with GST-β1 or different mutant forms of GST-β1 (Fig. 6*A*) and measured how this affected the ability of Arg to phosphorylate its substrate CrkII, as previously described (15). We found that although the K_m values did not significantly differ under the various conditions, preincubation of Arg with GST-β1 resulted in an enhancement of catalytic rate (k_{cat}) and an overall 2.34-fold increase in catalytic efficiency (k_{cat}/K_m) compared with Arg preincubated with control GST (Fig. 6, *B* and *C*). Mutation of either the Arg kinase domain-mediated interface (4KA) or the SH2-mediated interface (Y783F) significantly dampened this β1-mediated Arg activation (Fig. 6, *B* and *6C*). Preincubation with the integrin β3 tail did not enhance Arg kinase activation (data not shown), in agreement with our demonstration that Arg does not efficiently bind (8) or phosphorylate the β3 tail (Fig. 2*E*). These assays demonstrate that engagement of both the Arg kinase- and SH2-mediated interfaces promote enhancement of Arg kinase catalytic activity.

Integrin β1-Arg Interfaces Mediate Direct Interactions in Cells—Given the enhancement of Arg kinase activity by integrin β1 *in vitro* and in cells, we used FRET by FLIM to test whether the interaction interfaces we defined biochemically mediate interactions between these proteins in cells. *Integrin* $\beta1^{-/-}$ mouse embryonic fibroblasts expressing integrin β1-GFP alone or co-expressing Arg-mCherry were plated on fibronectin-coated glass for 45 min before donor GFP fluorescence lifetime was measured. Arg-mCherry expression led to a significant decrease in integrin β1-GFP donor lifetime as compared with control cells expressing integrin β1-GFP alone, indicating a direct interaction between β1-GFP and Arg-mCherry (Fig. 7, *A–C*). The observed FRET was predominantly concentrated at the cell periphery, consistent with the role we have previously defined for Arg in integrin-mediated dynamic cell edge protrusion (5, 7, 14, 38). We did not detect an interaction between integrin β1-GFP and cortactin-mCherry, a key Arg substrate in adhesion-dependent cell edge protrusion, indicating that integrin β1 interacts selectively with Arg in this assay (Fig. 7, *B* and *C*). These experiments indicate that integrin β1 interacts directly with Arg in fibroblasts during integrin-mediated adhesion and spreading.

We next evaluated which residues in integrin β1 and Arg mediate the direct interactions in cells. An RFP fusion to the Arg N-terminal half (N-term Arg, residues 1–557), which contains the SH3, SH2, and kinase domains, exhibited a strong FRET interaction with integrin β1-GFP during cell adhesion and spreading on fibronectin. In contrast, no significant interaction was observed between integrin β1-GFP and an Arg C-terminal half (C-term Arg, residues 557–1182) fused to RFP (Fig. 7, *D* and *E*). These results indicate that the Arg N-terminal half mediates a specific, direct interaction with β1 in adherent fibroblasts, consistent with our biochemical mapping of the β1-Arg interaction interfaces.

We engineered mutations in integrin β1-GFP to test whether disruption of the Arg kinase (4KA) interaction interface affected interactions with Arg-mCherry in cells. Interactions of Arg-mCherry with integrin 4KA-β1-GFP were significantly

FIGURE 7. **Arg interacts directly with integrin β1 in cells.** *A*, diagram of expression constructs used for FRET-FLIM assays and summary of the interaction results. *B*, Arg interacts directly with integrin β1 in cells. *Integrin* $\beta1^{-/-}$ mouse embryonic fibroblasts were transiently transfected with WT integrin β1-GFP alone or with Arg-mCherry or cortactin-mCherry and allowed to adhere and spread on fibronectin-coated coverslips for 45 min. FRET-FLIM analysis was performed, and fluorescence lifetimes are shown in the heat map corresponding to the values in the tau color scale legend. *C*, average FRET efficiencies for the direct Arg-β1 interaction. Data from three independent experiments, 8 cells/experiment/condition. *Error bars* represent S.E. from all 24 cells. *, $p < 0.05$. *D*, FRET was performed on *integrin* $\beta1^{-/-}$ mouse embryonic fibroblasts transiently co-transfected with WT β1-GFP with either Arg-RFP, N-term Arg-RFP, or C-term Arg-RFP and plated on fibronectin. Fluorescence lifetimes are shown in the heat map corresponding to the values in the tau color scale legend in *B*. Fluorescence lifetimes were calculated from two independent experiments of 10 cells/experiment/condition, and FRET efficiencies were quantified in *E* where *error bars* represent S.E. from all 20 cells. *, $p < 0.05$; **, $p < 0.01$. These experiments show that the Arg N-terminal half is necessary and sufficient to mediate interactions with integrin β1 in cells. *F*, Arg kinase- and SH2 domain-mediated interactions are both important mediators for the β1-Arg interaction in cells. *Integrin* $\beta1^{-/-}$ mouse embryonic fibroblasts were transiently co-transfected with WT integrin β1-GFP or 4KA β1-GFP, and Arg-mCherry or Arg R198K-mCherry and plated on fibronectin for 45 min, and FRET efficiencies were calculated from two independent experiments of nine cells/experiment/condition and reported in *G* where *error bars* represent S.E. from all 18 cells. **, $p < 0.01$; ***, $p < 0.001$. Fluorescence lifetimes are shown in the heat map corresponding to the values in the tau color scale legend in *B*. *H*, a model for Arg kinase activation by integrin β1. Upon integrin activation, Arg binds a lysine-rich region in the β1 tail through its kinase domain, and this partially activates Arg kinase activity. Arg can then phosphorylate the membrane-proximal Tyr-783 site on the integrin β1 tail, possibly in *cis* or *trans*, creating a second interface for the Arg SH2 domain. Engagement of these interaction interfaces enhances Arg kinase activation. *N-term*, N-terminal; *C-term*, C-terminal.

reduced compared with WT β1-GFP (Fig. 7, *F* and *G*), indicating that the Arg kinase domain-mediated interface promotes direct interactions with β1 in cells. We next tested the ability of an Arg SH2 domain interaction abrogating point mutant (R198K) (14) to bind β1-GFP or 4KA-β1-GFP. We found that in both cases the β1-Arg interaction was strongly abrogated upon introducing the Arg-R198K-mCherry mutant (Fig. 7, *F* and *G*). These data are consistent with a model in which the Arg kinase domain binds to the lysine-rich segment in integrin β1, partially activating Arg to promote Tyr-783 phosphorylation. Subsequently, the Arg SH2 domain engages the phosphorylated Tyr-783 region in the β1 tail, promoting further activation of the Arg kinase.

DISCUSSION

We provide evidence here that integrin β1 engages Arg via two distinct, direct interaction interfaces and that these interfaces mediate integrin β1-Arg interactions in cells and enhance Arg kinase activity. Abl family kinases are held inactive via a "latch-clamp-switch" mechanism where the Arg N-terminal cap, as well as its SH3 and SH2 domains, makes intramolecular interactions with the kinase domain (32, 39, 40). Structural and biochemical studies have shown that the SH2 domain makes a noncanonical interaction with the C-terminal lobe of the kinase domain, and the SH3 domain completes the inhibitory clamp by interacting with the SH2-kinase domain linker (32). These inhibitory intramolecular interactions limit kinase domain flexibility and are further latched by an interaction between the myristoylated N-terminal cap, or perhaps lipids in nonmyristoylated isoforms, with a hydrophobic pocket in the C-terminal lobe of the kinase domain (39). Previous reports have shown that ligands, such as the Ras effector protein Rin1, bind Abl family kinase SH3 and SH2 domains to unclamp the autoinhibitory switch (33, 34).

We report here that the Arg kinase domain interacts with a lysine-rich region in the integrin β1 tail, resulting in stimulation of Arg kinase activity (Fig. 7*H*). It is possible that kinase domain engagement of the lysine-rich motif in the β1 tail promotes allosteric Arg kinase activation by altering the conformation of the active site directly or indirectly through interaction with the SH2 domain-binding site or myristoyl binding pocket in the kinase domain C-terminal lobe. Future structural studies will be essential to further elucidate this activation mechanism at a high level of molecular detail.

Our work indicates that Arg phosphorylates the integrin β1 tail exclusively at the Tyr-783 site, and this event creates a second binding interface for interaction with the Arg SH2 domain. Our biochemical and FRET studies show that this interaction is a major driver of β1-Arg interactions in cells and serves to further enhance Arg kinase activity *in vitro*. This further enhancement in Arg kinase activation is quite likely due to the phosphorylated β1 tail sequestering interaction with the Arg SH2 domain away from its inhibitory intramolecular interaction with the Arg kinase domain C-terminal lobe (Fig. 7*H*). Further, although the inhibitory SH2-kinase domain interaction is atypical in that it is not mediated by a phosphotyrosine-containing sequence, the canonical ligand-binding site is partially occupied, and phosphotyrosine-containing peptides and ligands have been shown to compete for this interaction and activate kinase activity (33, 34, 40).

Using FRET-FLIM, we find that the Arg kinase and SH2 interaction interfaces mediate integrin β1-Arg interactions at the cell periphery, precisely where Arg kinase activity is required to phosphorylate adhesion proteins, such as cortactin and p190RhoGAP (4, 5). Therefore, this work provides a mechanistic framework to understand how direct engagement of an integrin activates the Abl family kinase Arg to control cytoskeletal structure and dynamics and drive cellular motility and morphogenesis behaviors.

Future work is needed to understand whether both integrin binding interfaces on Arg simultaneously engage the same integrin β1 tail or whether Arg can link two integrin tails together. Likewise, it will be important to determine whether and how these interactions control or are controlled by integrin clustering and how these interactions then affect β1 integrin localization. Indeed, Arg has been shown to function in regulating β1 localization, for example during establishment of epithelial cell polarity (41). Interestingly, Arg kinase activity was shown to be essential in promoting normal β1 integrin localization during this process (41). Finally, future work is needed to assess whether and how Arg competes with key integrin interactors such as talin to modulate integrin activation and localization.

Acknowledgments—We thank members of the Koleske and Calderwood labs for helpful discussions and Ke Zhang and Susana Wilson-Hawken for critical reading of the manuscript. We thank Xianyun Ye for technical support, Peter Davies for Arg antibodies, and Brian Rosenberg for purification of antibodies.

REFERENCES

1. Campbell, I. D., and Humphries, M. J. (2011) Integrin structure, activation, and interactions. *Cold Spring Harb. Perspect. Biol.* **3,** a004994–a004994
2. Lewis, J. M., Baskaran, R., Taagepera, S., Schwartz, M. A., and Wang, J. Y. (1996) Integrin regulation of c-Abl tyrosine kinase activity and cytoplasmic-nuclear transport. *Proc. Natl. Acad. Sci. U.S.A.* **93,** 15174–15179
3. Hernández, S. E., Settleman, J., and Koleske, A. J. (2004) Adhesion-dependent regulation of p190RhoGAP in the developing brain by the Abl-related gene tyrosine kinase. *Curr. Biol.* **14,** 691–696
4. Bradley, W. D., Hernández, S. E., Settleman, J., and Koleske, A. J. (2006) Integrin signaling through Arg activates p190RhoGAP by promoting its binding to p120RasGAP and recruitment to the membrane. *Mol. Biol. Cell* **17,** 4827–4836
5. Lapetina, S., Mader, C. C., Machida, K., Mayer, B. J., and Koleske, A. J. (2009) Arg interacts with cortactin to promote adhesion-dependent cell edge protrusion. *J. Cell Biol.* **185,** 503–519
6. Lewis, J. M., and Schwartz, M. A. (1998) Integrins regulate the association and phosphorylation of paxillin by c-Abl. *J. Biol. Chem.* **273,** 14225–14230
7. Miller, A. L., Wang, Y., Mooseker, M. S., and Koleske, A. J. (2004) The Abl-related gene (Arg) requires its F-actin-microtubule cross-linking activity to regulate lamellipodial dynamics during fibroblast adhesion. *J. Cell Biol.* **165,** 407–419
8. Warren, M. S., Bradley, W. D., Gourley, S. L., Lin, Y.-C., Simpson, M. A., Reichardt, L. F., Greer, C. A., Taylor, J. R., and Koleske, A. J. (2012) Integrin β1 signals through Arg to regulate postnatal dendritic arborization, synapse density, and behavior. *J. Neurosci.* **32,** 2824–2834
9. Moresco, E. M., Donaldson, S., Williamson, A., and Koleske, A. J. (2005) Integrin-mediated dendrite branch maintenance requires Abelson (Abl) family kinases. *J. Neurosci.* **25,** 6105–6118
10. Beaty, B. T., Sharma, V. P., Bravo-Cordero, J. J., Simpson, M. A., Eddy, R. J.,

Koleske, A. J., and Condeelis, J. (2013) β1 integrin regulates Arg to promote invadopodial maturation and matrix degradation. *Mol. Biol. Cell* **24,** 1661–1675, S1–S11
11. Peacock, J. G., Miller, A. L., Bradley, W. D., Rodriguez, O. C., Webb, D. J., and Koleske, A. J. (2007) The Abl-related gene tyrosine kinase acts through p190RhoGAP to inhibit actomyosin contractility and regulate focal adhesion dynamics upon adhesion to fibronectin. *Mol. Biol. Cell* **18,** 3860–3872
12. Kerrisk, M. E., Greer, C. A., and Koleske, A. J. (2013) Integrin α3 is required for late postnatal stability of dendrite arbors, dendritic spines and synapses, and mouse behavior. *J. Neurosci.* **33,** 6742–6752
13. Mader, C. C., Oser, M., Magalhaes, M. A., Bravo-Cordero, J. J., Condeelis, J., Koleske, A. J., and Gil-Henn, H. (2011) An EGFR-Src-Arg-cortactin pathway mediates functional maturation of invadopodia and breast cancer cell invasion. *Cancer Res.* **71,** 1730–1741
14. Miller, M. M., Lapetina, S., MacGrath, S. M., Sfakianos, M. K., Pollard, T. D., and Koleske, A. J. (2010) Regulation of actin polymerization and adhesion-dependent cell edge protrusion by the Abl-related gene (Arg) tyrosine kinase and N-WASp. *Biochemistry* **49,** 2227–2234
15. Tanis, K. Q., Veach, D., Duewel, H. S., Bornmann, W. G., and Koleske, A. J. (2003) Two distinct phosphorylation pathways have additive effects on Abl family kinase activation. *Mol. Cell. Biol.* **23,** 3884–3896
16. Boyle, S. N., Michaud, G. A., Schweitzer, B., Predki, P. F., and Koleske, A. J. (2007) A critical role for cortactin phosphorylation by Abl-family kinases in PDGF-induced dorsal-wave formation. *Curr. Biol.* **17,** 445–451
17. Parsons, M., Messent, A. J., Humphries, J. D., Deakin, N. O., and Humphries, M. J. (2008) Quantification of integrin receptor agonism by fluorescence lifetime imaging. *J. Cell Sci.* **121,** 265–271
18. Koleske, A. J., Gifford, A. M., Scott, M. L., Nee, M., Bronson, R. T., Miczek, K. A., and Baltimore, D. (1998) Essential roles for the Abl and Arg tyrosine kinases in neurulation. *Neuron* **21,** 1259–1272
19. Boyle, S. N., and Koleske, A. J. (2007) Use of a chemical genetic technique to identify myosin IIb as a substrate of the Abl-related gene (Arg) tyrosine kinase. *Biochemistry* **46,** 11614–11620
20. Moser, M., Legate, K. R., Zent, R., and Fässler, R. (2009) The tail of integrins, talin, and kindlins. *Science* **324,** 895–899
21. Wegener, K. L., Partridge, A. W., Han, J., Pickford, A. R., Liddington, R. C., Ginsberg, M. H., and Campbell, I. D. (2007) Structural basis of integrin activation by talin. *Cell* **128,** 171–182
22. García-Alvarez, B., de Pereda, J. M., Calderwood, D. A., Ulmer, T. S., Critchley, D., Campbell, I. D., Ginsberg, M. H., and Liddington, R. C. (2003) Structural determinants of integrin recognition by talin. *Mol. Cell* **11,** 49–58
23. Anthis, N. J., Wegener, K. L., Ye, F., Kim, C., Goult, B. T., Lowe, E. D., Vakonakis, I., Bate, N., Critchley, D. R., Ginsberg, M. H., and Campbell, I. D. (2009) The structure of an integrin/talin complex reveals the basis of inside-out signal transduction. *EMBO J.* **28,** 3623–3632
24. Harburger, D. S., Bouaouina, M., and Calderwood, D. A. (2009) Kindlin-1 and -2 directly bind the C-terminal region of beta integrin cytoplasmic tails and exert integrin-specific activation effects. *J. Biol. Chem.* **284,** 11485–11497
25. Arias-Salgado, E. G., Lizano, S., Shattil, S. J., and Ginsberg, M. H. (2005) Specification of the direction of adhesive signaling by the integrin beta cytoplasmic domain. *J. Biol. Chem.* **280,** 29699–29707
26. Arias-Salgado, E. G., Lizano, S., Sarkar, S., Brugge, J. S., Ginsberg, M. H., and Shattil, S. J. (2003) Src kinase activation by direct interaction with the integrin beta cytoplasmic domain. *Proc. Natl. Acad. Sci. U.S.A.* **100,** 13298–13302
27. Anthis, N. J., Haling, J. R., Oxley, C. L., Memo, M., Wegener, K. L., Lim, C. J., Ginsberg, M. H., and Campbell, I. D. (2009) Beta integrin tyrosine phosphorylation is a conserved mechanism for regulating talin-induced integrin activation. *J. Biol. Chem.* **284,** 36700–36710
28. Bledzka, K., Bialkowska, K., Nie, H., Qin, J., Byzova, T., Wu, C., Plow, E. F., and Ma, Y.-Q. (2010) Tyrosine phosphorylation of integrin beta3 regulates kindlin-2 binding and integrin activation. *J. Biol. Chem.* **285,** 30370–30374
29. Morse, E. M., Brahme, N. N., and Calderwood, D. A. (2014) Integrin cytoplasmic tail interactions. *Biochemistry* **53,** 810–820
30. Yang, J., Campobasso, N., Biju, M. P., Fisher, K., Pan, X.-Q., Cottom, J., Galbraith, S., Ho, T., Zhang, H., Hong, X., Ward, P., Hofmann, G., Siegfried, B., Zappacosta, F., Washio, Y., Cao, P., Qu, J., Bertrand, S., Wang, D.-Y., Head, M. S., Li, H., Moores, S., Lai, Z., Johanson, K., Burton, G., Erickson-Miller, C., Simpson, G., Tummino, P., Copeland, R. A., and Oliff, A. (2011) Discovery and characterization of a cell-permeable, small-molecule c-Abl kinase activator that binds to the myristoyl binding site. *Chem. Biol.* **18,** 177–186
31. Nagar, B., Hantschel, O., Seeliger, M., Davies, J. M., Weis, W. I., Superti-Furga, G., and Kuriyan, J. (2006) Organization of the SH3-SH2 unit in active and inactive forms of the c-Abl tyrosine kinase. *Mol. Cell* **21,** 787–798
32. Nagar, B., Hantschel, O., Young, M. A., Scheffzek, K., Veach, D., Bornmann, W., Clarkson, B., Superti-Furga, G., and Kuriyan, J. (2003) Structural basis for the autoinhibition of c-Abl tyrosine kinase. *Cell* **112,** 859–871
33. Hantschel, O., Nagar, B., Guettler, S., Kretzschmar, J., Dorey, K., Kuriyan, J., and Superti-Furga, G. (2003) A myristoyl/phosphotyrosine switch regulates c-Abl. *Cell* **112,** 845–857
34. Cao, X., Tanis, K. Q., Koleske, A. J., and Colicelli, J. (2008) Enhancement of ABL kinase catalytic efficiency by a direct binding regulator is independent of other regulatory mechanisms. *J. Biol. Chem.* **283,** 31401–31407
35. Fox, J. E., Lipfert, L., Clark, E. A., Reynolds, C. C., Austin, C. D., and Brugge, J. S. (1993) On the role of the platelet membrane skeleton in mediating signal transduction. Association of GP IIb-IIIa, pp60c-src, pp62c-yes, and the p21ras GTPase-activating protein with the membrane skeleton. *J. Biol. Chem.* **268,** 25973–25984
36. Oser, M., Yamaguchi, H., Mader, C. C., Bravo-Cordero, J. J., Arias, M., Chen, X., Desmarais, V., van Rheenen, J., Koleske, A. J., and Condeelis, J. (2009) Cortactin regulates cofilin and N-WASp activities to control the stages of invadopodium assembly and maturation. *J. Cell Biol.* **186,** 571–587
37. Campbell, D. H., Sutherland, R. L., and Daly, R. J. (1999) Signaling pathways and structural domains required for phosphorylation of EMS1/cortactin. *Cancer Res.* **59,** 5376–5385
38. Gifford, S. M., Liu, W., Mader, C. C., Halo, T. L., Machida, K., Boggon, T. J., and Koleske, A. J. (2014) Two amino acid residues confer different binding affinities of Abelson family kinase Src homology 2 domains for phosphorylated cortactin. *J. Biol. Chem.* **289,** 19704–19713
39. Bradley, W. D., and Koleske, A. J. (2009) Regulation of cell migration and morphogenesis by Abl-family kinases: emerging mechanisms and physiological contexts. *J. Cell Sci.* **122,** 3441–3454
40. Harrison, S. C. (2003) Variation on an Src-like theme. *Cell* **112,** 737–740
41. Li, R., and Pendergast, A. M. (2011) Arg kinase regulates epithelial cell polarity by targeting β1-integrin and small GTPase pathways. *Curr. Biol.* **21,** 1534–1542